Transaction of the Korean Society of Mechanical Engineers, Vol. 10, No. 6, pp. 947~958, 1986.

<Original>

Local Mean Water Layer Thickness in Countercurrent Stratified Two-Phase Flow

Hho Jung Kim* and Kap Kim*

(Received March 13, 1986)

물-증기 역류 성층이상유동에서의 국부 평균 액체층 두께

김 효 정·김 갑

Key Words: Falling Film(낙하 액체막), Probability Distribution(확률 분포), Mixing Length Theory(혼합길이 이론), Time-Mean Film Thickness(시간평균 액체막 두께), Volume-Average Film Thickness(체적평균 액체막의 두께), Wave Trough(파곡)

초 록

물-증기 역류 성층이상유동에서의 평균 액체층 두께가 여러가지 경사각과 종횡비에 따라 측정되었다.

난류유동에 있어서 전단응력분포의 선형화와 von Karman의 혼합길이 이론을 근거로 평균 액체층의 두께에 대한 관계식이 제시되었으며 실험결과와 잘 일치하였음을 보였다. 접촉면에서의 조파저항이 고려되지 않은 해석결과는, 수평 성층유동의 경우에, 평균 액체층 두께보다는 오히려 파곡까지의 액체층 두께를 예측하고 있는 것으로 나타났다.

또한 평균 액체층 두께에 대한 실험 상관관계식이 계산시 편의를 위해 쉽게 인지할 수 있는 매개변수들의 항들로 제시되었다.

Nomenclature

b	: Dimensionless length scale, $u_*\delta/\nu$
C	: Constant
f	: Friction coefficient
Fr	: Froude number
g	: Acceleration of gravity
H	: Channel height
P	: Static pressure, Probability
Q	: Volumetric flow rate per unit width
Re	: Reynolds number
u	: Streamwise velocity
$\bar{u}$	: Average velocity
u_1	: Velocity at y_1
u_2	: Velocity at y_2
u^+	: Dimensionless velocity scale, u/u_*
u_*	: Shear velocity
X	: Parameter
y	: Coordinate normal to flow
y_1	: Thickness of viscous sublayer

* Member, Korea Advanced Energy Research Institute

y_2 : Point of zero shear stress
y^+ : Dimenisonless length scale, $u_* y/\nu$
y' : Dimensionless length scale, y/δ
z : Distance from water inlet
α : Void fraction
β : Ratio of gravity force to wall shear stress
γ : Ratio of gravity force to interfacial shear stress
δ : Mean water layer thickness
δ' : Dimensionless water layer thickness
θ : Inclination angle in degree
κ : von Karman constant
μ : Viscosity
ν : Kinematic viscosity
ρ : Density
τ : Shear stress

Subscripts

b : Upper wall surface
E : Eddy
f : Liquid phase
g : Gas phase
i : Interface
o : Liquid wall surface

1. Introduction

An understanding of the mechanics of film flow is important in those cases of heat and mass transfer which involve two-phase flow. Flow in vertical condensers, film reactors, water tube boilers operating at high flow rates, and packed towers are a few practical examples of this flow configuration. This study of liquid thickness was undertaken in order to define more fully the liquid-film conditions so that the analysis of two-phase flow could be made on a rational basis and ultimately be extended to the transfer process.

In condensation, the transfer coefficient and the interfacial transfer area are the important factors to affect the transfer rate. Especially transfer area depends on the wave motion at the steam-water interface and on the liquid layer thickness.

Although a considerable literature exists on the thickness of falling films in cocurrent gas-liquid flow, or in liquid-only flow, the literature for inclined stratified countercurrent flow is much more sparse.

It is generally known that as the gas velocity is increased, resulting in an increase of the interfacial shear stress, the water layer thickness for a given liquid flow rate decreases for cocurrent flow, due to the acceleration of the liquid surface by the interfacial shear, whereas for countercurrent flow the opposite effect occurs, due to the deceleration of the liquid surface.

A simplified relation for the water layer thickness is developed here for the turbulent liquid flow, with or without the interfacial shear stress acting in the opposite direction to the liquid flow.

2. Analytical Approach

It is useful to attempt to develop the analytical approach for steady-state, turbulent, stratified, countercurrent flow with or without condensation.

2.1 Thickness of Water Layer without Interfacial Shear

The volumetric flow rate per unit width in a falling film can be calculated using a universal velocity distribution:

$$Q=\bar{u}\cdot\delta=\int_0^\delta u\ dy=\nu\int_0^b u^+\ dy^+ \qquad (1)$$

The von Karman[1] universal distribution is defined by:

$$u^+=y^+ \qquad 0<y^+<5 \qquad (2)$$

$$u^+=-3.05+5.0\ \ln\ y^+ \qquad 5<y^+<30 \qquad (3)$$

$$u^+=5.5+2.5\ \ln\ y^+ \qquad 30<y^+<b \qquad (4)$$

Assuming that these equations, which were written for fully-developed pipe flow, can be applied to the liquid phase in two-phase flow, it is possible to develop a relationship between the film thickness and the flow rate. Gazley[2] examined the flow of air over a flat plate on a universal basis, and demonstrated that the constants and form of the equation for the velocity distribution in the turbulent boundary layer were almost identical to Eq. (4). This model has also been used successfully by Dukler and Bergelin[3] for falling liquid films in a vertical channel, by Roshenow, et al[4] for turbulent film condensation on vertical plates, and by Linehan[5] for cocurrent horizontal liquid film flow in a rectangular channel; a more detailed discussion of this assumption has been given by Dukler and Bergelin[3].

This integration gives:

$$Q/\nu=b\{3.0+2.5\ \ln\ b\}-64 \qquad (5)$$

The wall shear stress in the absence of interfacial shear is given by:

$$\tau_0=\rho\cdot g\ \sin\ \theta\cdot\delta \qquad (6)$$

In the above equations, the friction velocity and the dimensionless film thickness are defined by:

$$u_*=\sqrt{\tau_0/\rho}=\sqrt{\delta\cdot g\ \sin\theta} \qquad (7)$$

$$b=u_*\cdot\delta/\nu=\{g\ \sin\theta/\nu^2\}^{\frac{1}{2}}\ \delta^{\frac{3}{2}} \qquad (8)$$

Substituting Eq. (8) into Eq. (5) and rearranging the terms:

$$\delta=\left(\frac{\nu^2}{g\cdot\sin\theta}\right)^{\frac{1}{3}}\left(3.0+2.5\ln\frac{\delta u_*}{\nu}\right)^{-\frac{2}{3}}\left(1+\frac{64}{Re}\right)^{\frac{2}{3}}Re^{\frac{2}{3}} \qquad (9)$$

If the minimum value for the turbulent Reynolds number is assumed to be 400, one has:

$$(1+64/Re)^{\frac{2}{3}}\approx 1+2/3(64/Re) \qquad (10)$$

Substituting Eq. (10) into Eq. (9), one obtains:

$$\delta=\frac{1+42.3Re^{-1}}{\left(3.0+2.5\ln\frac{\delta\cdot u_*}{\nu}\right)^{\frac{2}{3}}}\left(\frac{\nu^2}{g\cdot\sin\theta}\right)^{\frac{2}{3}}Re^{\frac{2}{3}} \qquad (11)$$

To get the relation between u and u_*:

$$\tau_0=f\rho u^2/2 \qquad (12)$$

The wall shear stress may be calculated from the Blasius equation for the friction factor in turbulent flow, which is defined as:

$$f_b=0.079\,Re^{-0.25} \qquad (13)$$

Substituting Eq. (13) into Eq. (11), and defined the dimensionless parameter X, one obtains:

$$X=\frac{1+42.3\cdot Re^{-1}}{\left(3.0+2.5\ln\frac{\delta\cdot u_*}{\nu}\right)^{\frac{2}{3}}}=\frac{1+42.3\cdot Re^{-1}}{(3.0+2.5\ln\sqrt{0.028\cdot Re^{-1/4}}+2.5\ \ln Re)^{\frac{2}{3}}} \qquad (14)$$

The parameter, X, is a weak function of the Reynolds number:

$$X\approx 0.375Re^{-0.105} \qquad (15)$$

Substituting Eq. (15) into Eq. (11) ;

$$\delta'=\frac{\delta}{\left(\frac{\nu^2}{g\cdot\sin\theta}\right)^{\frac{1}{3}}}=0.375\left(\frac{\nu^2}{g\cdot\sin\theta}\right)^{\frac{1}{3}}Re^{0.562} \qquad (16)$$

This provides a very simple relation between the film thickness and the flow rate. Alternatively, the film thickness can be obtained by using Eq. (5) with information on the wall shear stress.

This final relation (Eq. (16)) has the same form as the equations obtained by several investigators for free-falling turbulent wall layers, even though the constants and exponents are somewhat different:

$$\delta'=0.435\,Re^{8/15}\ \text{Brauer}[6] \qquad (17)$$

$$=0.172\,Re^{2/3}\ \text{Brotz}[7] \qquad (18)$$

$$=0.532\,Re^{1/2}\ \text{Feind}[8] \qquad (19)$$

$$=0.316\,Re^{7/12}\ \text{Zhivaikin, et al.}[9] \qquad (20)$$

$$=0.473\,Re^{0.526}\ \text{Takahama, et al.}[10] \qquad (21)$$

A detailed discussion of these correlations

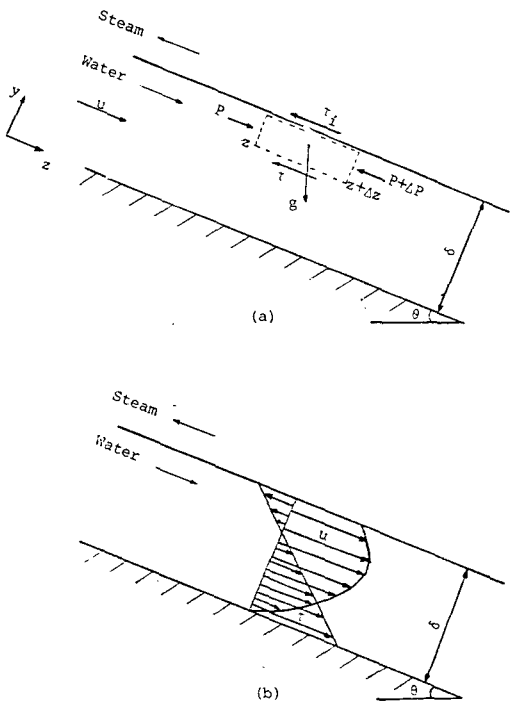

(a) Liquid flow element
(b) Expected velocity & shear stress distribution

Fig. 1 Assumed flow characteristics in water layer

has been given by Fulford[11]. It is of value to compare the present data, which have been obtained for a variety of inclination angles but in the absence of interfacial shear stress, with Eq. (16), as well as these correlations for further analysis.

2.2 Thickness of Water Layer with Interfacial Shear

From a force balance for the control volume in a liquid flow system (Fig. 1), one obtains:

$$\tau=(\rho\cdot g\sin\theta-\Delta p/\Delta z)(\delta-y)-\tau_i \quad (22)$$

Assuming $\rho\cdot g\sin\theta\gg\frac{\Delta p}{\Delta z}$, the equation for the distribution of shear stress can be obtained:

$$\tau=\rho\cdot g\sin\theta(\delta-y)-\tau_i \quad (23)$$

From the above equation,

$$\tau_0=\rho\cdot g\sin\theta\cdot\delta-\tau_i \quad (24)$$

The shear stress is related to the velocity gradient by:

$$\tau=\rho(\nu+\nu_E)du/dy \quad (25)$$

The relation between the shear stress and the velocity gradient is defined, using the Prandtl mixing length theory and neglecting the kinematic viscosity:

$$\tau=\rho\kappa^2y^2|du/dy|du/dy \quad (26)$$

where κ is the von Karman constant(=0.4). Combining Eq. (23) and (26);

$$\rho\kappa^2y^2|du/dy|du/dy=\rho\cdot g\sin\theta(\delta-y)-\tau_i \quad (27)$$

When $y_2=\delta-\tau_i/(\rho\cdot g\sin\theta)$, the shear stress is zero and the slope of the velocity distribution is reversed.

The velocity distribution is solved separately in three regimes. In the region of viscous sublayer, where $0<y<y_1$,

$$\rho\cdot g\sin\theta(\delta-y)-\tau_i=\mu du/dy \quad (28)$$

By integrating, the velocity at y_1 can be obtained:

$$u_1=\frac{1}{\mu}\{(\rho\cdot g\sin\theta\cdot\delta-\tau_i)y_1-\rho\cdot g\sin\theta y_1^2/2\} \quad (29)$$

The thickness of the viscous sublayer, y_1, is obtained from:

$$y_1=C\nu/u_*=11.6/\sqrt{\tau_0/\rho} \quad (30)$$

Where the value of 11.6 has been taken for the value of the constant, C[12].

In the region ($y_1<y<y_2$) where the shear stress is positive, Eq. (27) is solved by substituting:

$$\rho\kappa^2y^2(du/dy)^2=\rho\cdot g\sin\theta(\delta-y)-\tau_i \quad (31)$$

Taking the square root, integrating once and inserting the boundary condition:

$$u=u_1 \text{ at } y=y_1;$$

$$u=u_1+\sqrt{\frac{\tau_0/\rho}{\kappa}}\left\{2(\sqrt{1-\beta\cdot y'}-\sqrt{1-\beta\cdot y_1'})+\ln\frac{\sqrt{1-\beta\cdot y'}-1}{\sqrt{1-\beta\cdot y_1'}-1}+\ln\frac{\sqrt{1-\beta\cdot y_1'}+1}{\sqrt{1-\beta\cdot y'}+1}\right\} \quad (32)$$

In the region ($y_2<y<\delta$) where the shear

stress is negative, Eq. (27) is solved by substituting:

$$\rho\kappa^2(\delta-y)^2(du/dy)^2=-\{\rho\cdot g\sin\theta(\delta-y)-\tau_i\} \tag{33}$$

This yields:

$$u=u_2+\frac{\sqrt{\tau_0/\rho}}{\kappa}\left\{2(\sqrt{-1+\beta\cdot y'}-\sqrt{-1+\beta\cdot y_2'})+\sqrt{-1+\beta}\left(\ln\frac{\sqrt{-1+\beta\cdot y'}-\sqrt{-1+\beta}}{\sqrt{-1+\beta\cdot y_2'}-\sqrt{-1+\beta}}+\ln\frac{\sqrt{-1+\beta\cdot y_2'}+\sqrt{-1+\beta}}{\sqrt{-1+\beta\cdot y'}+\sqrt{-1+\beta}}\right)\right\} \tag{34}$$

The quantity of liquid flowing through the film can be calculated from:

$$Q=\int_0^{\delta}u\,dy=\int_0^{y_1}u\,dy+\int_{y_1}^{y_2}u\,dy+\int_{y_2}^{\delta}u\,dy \tag{35}$$

These relationships allow calculation of the liquid film thickness from a knowledge of the liquid flow rate and the interfacial shear stress. The interfacial shear stress can be calculated by means of adding the condensation induced shear stress to the interfacial shear stress in the absence of condensation. The details can be found in reference[13]. The velocity distributions obtained from Eqs. (29), (32) and (34) are shown in Fig. 2, as functions of the dimensionless interfacial shear stress $\gamma=\tau_i/(\rho\cdot g\sin\theta\cdot\delta)$. As expected, the interface velocity becomes smaller as the interfacial shear stress increases. The relation between the dimensionless film thickness and the Reynolds number is shown in Fig. 3. Again as expected, the film thickness increases as the interfacial shear stress increases, in contrast to cocurrent flow.

One can note, in Fig. 3, that the derived relation for $\gamma=0$ is numerically indistinguishable from Eq. (16), which has been derived directly from the von Karman velocity distribution and the Blasius friction formula, thus substantiating the consistency of the assumptions.

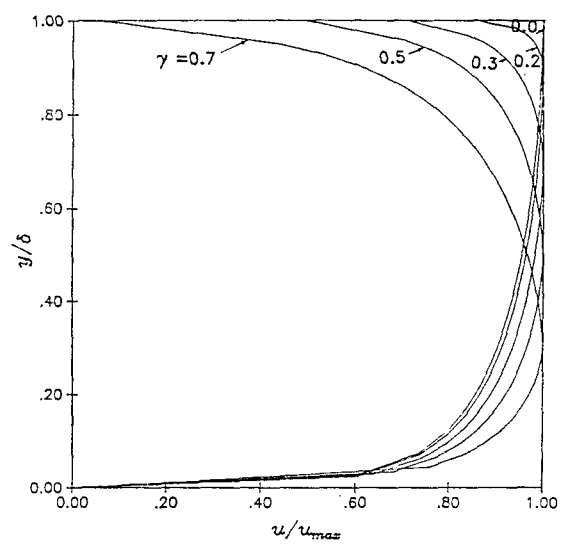

Fig. 2 Liquid velocity profiles depending on interfacial shear stress

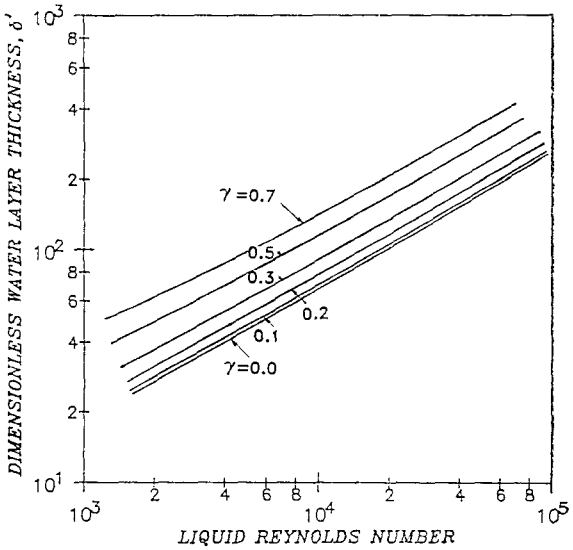

Fig. 3 Relation between δ' and Re_f depending on interfacial shear stress

3. Experimental Procedure

The steam-water countercurrent flow contactor is made up of three sections, consisting of an upper and a lower plenum, together with a test section, as shown in Fig. 4.

The upper and the lower plena are designed

to insure smooth exit and entry of steam and water. The test section is provided with the appropriate instrumentation to determine the locae steam flow rate and interfacial wave structure. The test section is completely insulated except for pyrex windows fitted into both side plates for visual observation. Liquid entry is through a porous stainless steel plate, with thickness 2.4mm and porosity 100 microns. For water flow rates of 0.3~3.0kg/s, the pressure drop through the porous medium is 170~200kg/m², which is adequate to establish a smooth gravity-fed flow at the liquid entrance of the test section. The steam entrance region in the lower plenum contains a set of screens and a perforated plate to establish uniform flow. In addition, honeycomb material is inserted to act as turning vanes through the 90° bend. The inlet water temperature can be controlled to any desired temperature by means of a heat exchanger. Steam from the building supply is throttled down to a slightly superheated temperature at atmospheric pressure after removing any condensate in the supply line by means of a steam separator.

The steam flow rates were measured at six

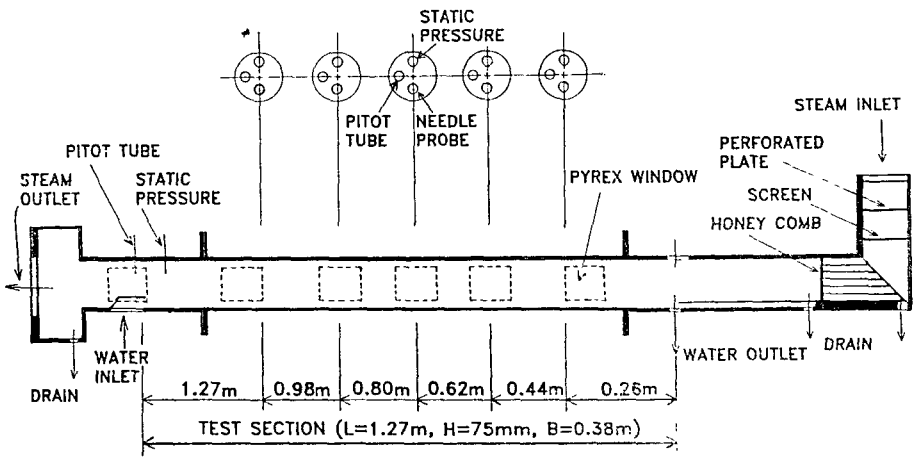

Fig. 4 Sketch of test section

Table 1 Dimension of test section and experimental flow range

Data set		A	B	C	D
Inclination angle (θ)		4	30	87	33
Width $B(m)$		0.38	0.38	0.38	0.38
Height $H(m)$		0.075	0.075	0.075	0.038
Length $L(m)$		1.27	1.27	1.27	1.27
Aspect Ratio, B/H		5	5	5	10
Measuring Station(m), from Steam inlet	1	0.26	0.26	0.22	0.22
	2	0.44	0.44	0.40	0.40
	3	0.62	0.62	0.58	0.58
	4	0.80	0.80	0.76	0.76
	5	0.98	0.98	0.93	0.93
	6	1.27	1.27	1.27	1.27
Re_x		2500~30000	5000~30000	3000~20000	3000~18000
Re_f		800~15000	1000~ 8000	800~ 7000	800~ 5000

stations along the channel centerline: the distance of each station from the steam entrance is given in Table 1. This was accomplished by integrating the measured steam velocity profile at each station, assuming two-dimensional flow. The two-dimensionality assumption was verified by pitot tube traverses across the width of the test section, and the integration method was checked by measuring the steam velocity profiles across the heights of the test section with zero water flow. Upon comparing the measured inlet steam flow rate with the calculated local steam flow rate, it was found that the deviation was less than 2%. The pitot tubes, which were electrically heated to prevent steam from condensing inside the tubes, were attached to a common traversing table, allowing them to be positioned at selected elevations in the test section within 0.05mm. The difference between total and static pressure for each pitot tube was measured by means of diaphragm-type differential pressure transducer. The inlet steam flow rate was calculated from measurements of the differential pressure, absolute pressure and the thermodynamic state of the incoming steam, using a 50mm inlet steam venturi. Inlet and outlet temperatures of the steam and water were measured by using K-type (Chromel-Alumel) thermocouples connected to a zero-point reference junction. The inlet water flow rate was determined by measuring the pressure drop across a 32mm water venturi meter.

Even though a large variety of techniques has been developed for the determination of the interfacial wave structure[14,15], needle contact probes have been adopted for the present research because of the relatively thick films, as well as the presence of condensation.

These probes tend to underestimate the void fraction in bubbly flows because of deflection of the bubbles before and upon hitting the probe, in view of their low effective mass. However, this problem appears to be minimal in measuring interfacial waves with small-diameter probes. Another serious difficulty in the application of this type of probe is the uncertainty about contact hysteresis. It is possible for the probe to remain in extended contact with the liquid by dragging out a filament of liquid before a break in contact is recorded. These problems can lead to rise and fall times which are comparable to the contact times, and hence require trigger circuits with arbitrarily chosen gating voltages for measuring the local phase fraction. In addition to this problem, polarization effects and electrochemical attack of the probe must be avoided.

To minimize these effects, the probe, consisting of a 0.5mm stainless steel needle with a sharpened tip, was made non-wetting by application of a teflon coating, except at the very tip. A.C. excitation at 10kHz is used to avoid the polarization problem. To obtain an accurate position of the probe tip relative to the bottom wall, the probe is traversed by means of a

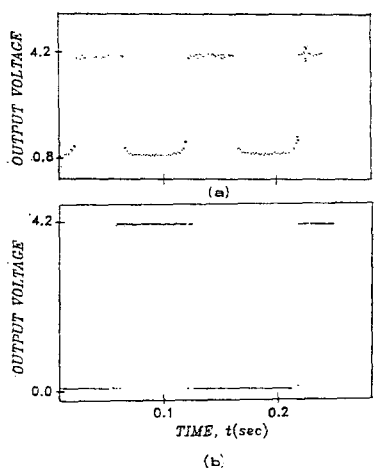

(a) at gas-liquid interface
(b) at gas-solid interface

Fig. 5 Typical signal obtained from needle contact probe

micrometer attachment, first to the wall, and then returned to the interface. In practice, the raw probe output was quite close to a series of step functions, so that the distribution of probability for liquid contact with the probe as a function of probe elevation could be measured without resorting to trigger circuits. The probability is equivalent to the time-average liquid volume fraction, $1-\alpha$, as a function of height.

The probe signals were fed directly into a PDP-11/34 computer through an A/D converter with, usually, a sampling time and sampling frequency of about 5 seconds and 2000 Hz. The signal obtained through A.C. circuitry by the teflon-coated probe at the gas-liquid interface is shown in Fig. 5, and compared with the signal from the contact of the probe with the solid metal.

The range of test conditions was restricted for two reasons: (i) high water and/or steam flow rates produce surface instabilities, leading to bridging and/or flooding; (ii) with cold water and low steam flow rates, complete condensation occurs within the test section, which results in large pressure pulses (water hammer). For these reasons, the experimental ranges in the present geometry were quite limited; the ranges of the gas and liquid Reynolds number for various inclination angles and aspect ratios are given in Table 1.

4. Results and Discussion

The mean water layer thicknesses were calculated from probability distributions which were obtained by traversing micrometer-mounted needle contact probes, as described in Section 3. Typical data for probability distribution as a function of probe heights are shown in Fig. 6. The mean water layer thickness was obtained using the probability distribution function and defined by:

$$\delta=\int_0^1 y(P)\ dP \tag{36}$$

The slopes in the mean water layer thickness have wide variations, depending on inlet flow conditions. In general, the mean water layer thickness has an increasing slope along

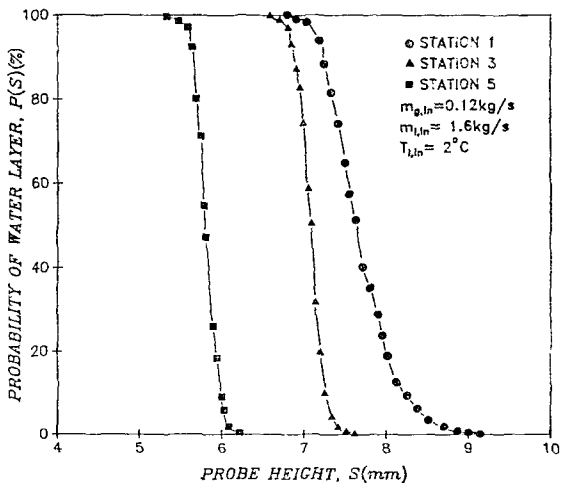

Fig. 6 Probability distribution at different stations

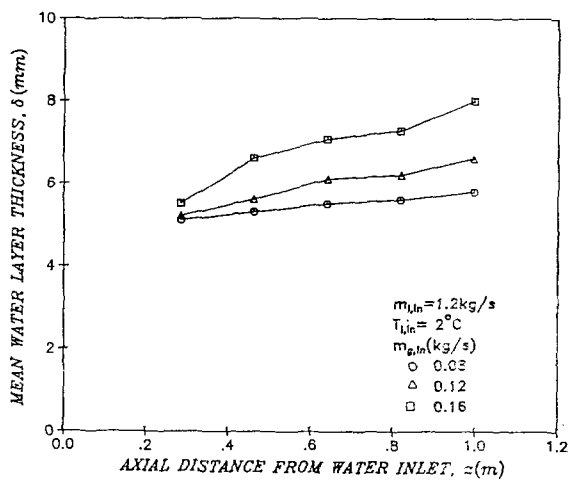

Fig. 7 Axial mean water layer thickness profile as a function of inlet steam flow rate

the direction of flow with increasing inlet water and steam flow rates, as shown in Fig. 7 with typical data, which exhibits characteristics similar to the condensation rates and interfacial shear stress[16]. The increase in condensation rates with increasing steam and water flow rates results in increase in the interfacial shear stress, which is attributed to the increase in water layer thickness. As the inlet water temperature increases, the slope of the water layer thickness becomes flat. In particular, at almost saturated inlet water temperatures where the condensation rates can be negligible, the water layer thickness is almost the same through the whole channel. This is attributed to the uniform distribution of local flow properties, depending on the inlet flow conditions in the absence of heat and mass transfer. This result suggests reasonable verification for using local flow properties in finding turbulent correlations.

An equation for the water layer thickness was derived by using Prandtl mixing length theory and the turbulent transport equation for the relation between the shear stress and the velocity gradient, and assuming a linear distribution of shear stress in the water layer, either with or without the interfacial shear stress.

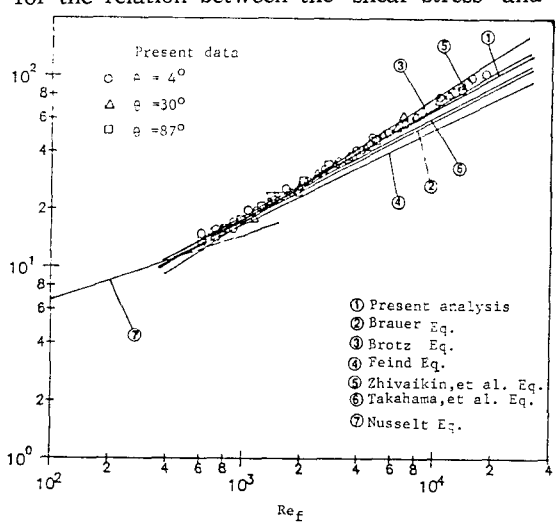

Fig. 8 Comparison of measured water layer thickness with correlations without interfacial shear stress

The non-dimensional form of Eq. (16), with zero interfacial shear stress, is compared with the correlations for free-falling turbulent wall layers, as well as the Nusselt equation for laminar film flow, described above. These relationships are also compared with experimental data at several inclination angles, in the absence of the interfacial shear stress, in Fig. 8. The dimensionless film thickness, δ', varies with some power of the liquid Reynolds number between 1/2 and 2/3, except for the laminar film flow. It can be further seen that, at the Reynolds numbers from 600~2000, there is little difference between the values predicted by these correlations. This may arise from the fact that these correlations are obtained in similar ranges of liquid Reynolds numbers; the liquid Reynolds number varies from 400~1800 in the Brauer correlation, 590~4300 (Brotz), 400~2100 (Feind), 400~3500 (Zhivaikin, et al.) and 300~2000 (Takahama, et al.). The experimental data agree well with the present analysis, even though somewhat underestimated at high Reynolds numbers. At high Reynolds numbers, the interface is characterized by waves with finite amplitude. Wave deformation and nonlinear effects become important for these large waves, which may account for this deviation. It is interesting to note that the Zhivaikin, et al. correlation, which was obtained for the vertical film flow in a circular tube, shows a similar trend as the present analysis, and fairly well corresponds to the present data, which were obtained in the rectangular channel flow for several inclination angles.

The water layer thicknesses in the presence

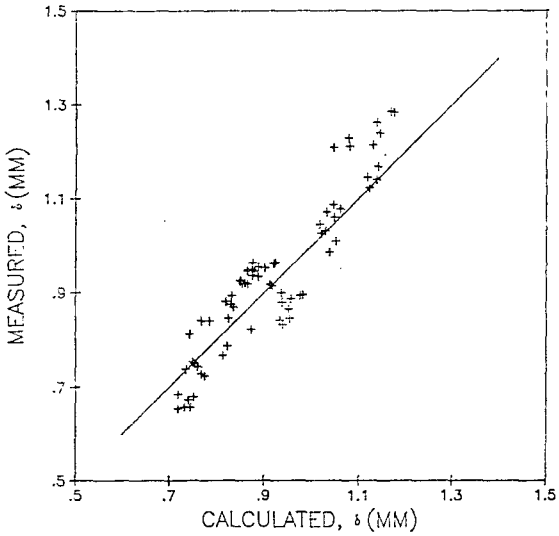

Fig. 9 Comparison of measured mean water layer thickness with the calculated value with interfacial shear stress at a nearly vertical inclination ($\theta=87°$)

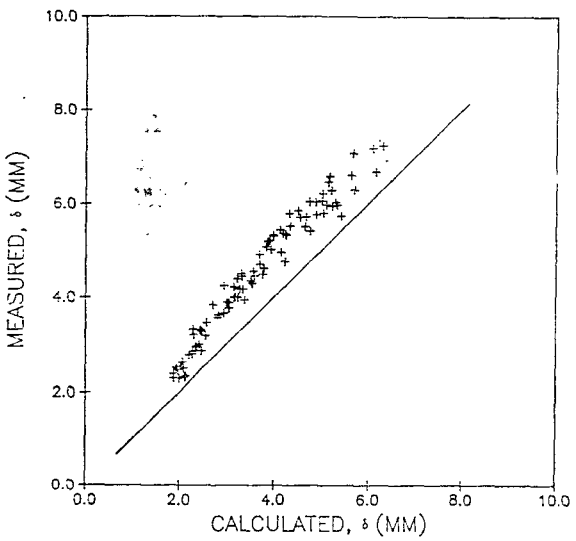

Fig. 10 Comparison of measured mean water layer thickness with the calculated value with interfacial shear stress at a nearly horizontal inclination ($\theta=4°$)

of the interfacial shear stress were calculated, using the method described in Section 2, according to the dimensionless interfacial shear stress, γ, and compared with the measured water layer thickness. For the nearly vertical angle ($\theta=87°$), the calculated water layer thicknesses are in good agreement with the measured mean water layer thicknesses, as shown in Fig. 9. On the other hand, for the nearly horizontal angle ($\theta=4°$), the calculated thicknesses are smaller than the measured mean thicknesses, as shown in Fig. 10. This discrepancy may be attributed to significant wave structure differences at different inclination angles. For the nearly horizontal countercurrent flow, it was observed that the interface is characterized by the presence of three-dimensional pebbly waves. The measured thicknesses are obtained from the Eq. (36), which is nearly identical to the point where $\alpha=0.5$[13]. Since the equation for the thickness was derived neglecting the wave structure, it is questionable whether the point where $\alpha=0.5$, which corresponds to the local time-mean film thickness, would be the same as the local volume-average film thickness. Another point is that, for the nearly horizontal countercurrent flow, the interface velocity becomes greatly decelerated, owing to the gas stream drag and the relatively small gravity force, as the gas stream velocity is inceased. Therefore, the interface in this case can be considered to be nearly stagnant with a finite-amplitude wave. Large lumps of liquid, which carry a significant portion of the total liquid flow, move down the inferface with no change in interface shape. Hence the smooth film velocity distribution analysis will predict primarily the thickness of the wave trough, rather than the mean film thickness. This is recognized in the comparison of the calculated thicknesses with the measured thicknesses of the wave trough, as shown in Fig. 11, resulting in good agreement.

As an alternate approach, it is useful to correlate the mean water layer thickness in terms of local flow properties. In order to

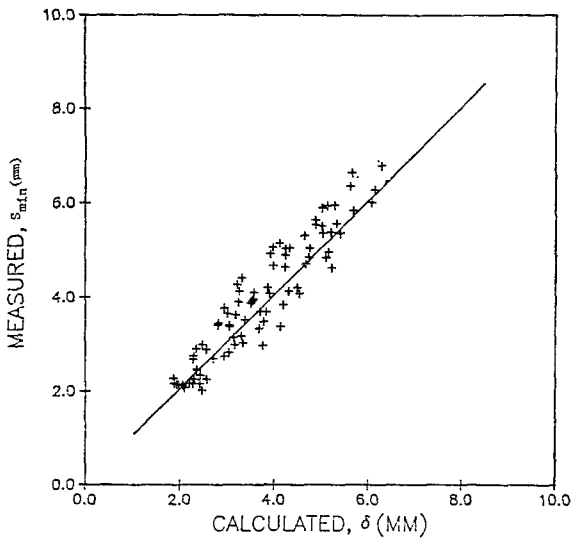

Fig. 11 Comparison of measured thickness of wave trough with the calculated value with interfacial shear stress at a nearly horizontal inclination ($\theta=4°$)

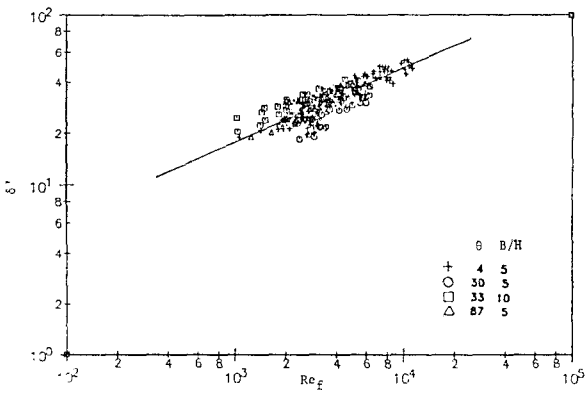

Fig. 12 Experimental correlation for mean water layer thickness comprising whole body of data

obtain a general empirical correlation, all the dimensionless water layer thickness data were correlated as a function of the inclination angle, liquid Reynolds number and Froude number, which corresponds to the effect of the gas stream. Using a least-square fit, this gives:

$$\delta'=0.882Re_f^{0.44}Fr^{0.37}(\cos\theta)^{0.1} \qquad (37)$$

where $Fr=\bar{u}_g/\sqrt{g(H-\delta)}$

The data fit Eq. (37) fairly well with a standard deviation of 14%, as shown in Fig.12.

In addition to the present analysis for the water layer thickness, described in Section 2, either with or without the interfacial shear stress, the relationship (Eq. (37)) can be tentatively recommended as a guide to predict the mean water layer thickness in the presence of the interfacial shear stress, since this relationship is composed of easily accessible parameters.

5. Conclusions

The measurement of mean water layer thickness has been performed for a countercurrent, stratified, steam and water flow, at various inclination angles and aspect ratios. The slopes in the mean water layer thickness have wide variations. In general, the mean water layer thickness has an increasing slope along the direction of flow with increasing inlet water and steam flow rates, which exhibits characteristics similar to the condensation rates and interfacial shear stress.

The mean water layer thicknesses were calculated by assuming a linear shear stress distribution and using the von Karman mixing length hypothesis. The calculated thicknesses were compared with the experimental data, resulting in a good agreement. The smooth-film velocity distribution analysis is shown to predict primarily the film thickness up to the wave troughs, rather than the mean film thickness, for the nearly horizontal flow.

In an alternate approach, the experimental correlation [Eq. (37)], which is composed of easily accessible parameters, is suggested as a guide to predict the mean water layer thickness.

References

(1) von Karman, T., "The Analogy Between Fluid Friction and Heat Transfer," Trans. ASME, Vol. 61, pp. 705~710, 1939

(2) Gazley, C., "Co-current Gas-Liquid Flow in Horizontal Tubes," Proc. Heat Trans. and Fluid Mech. Inst.; p. 29, 1949

(3) Dukler, A.E. and Bergelin, O.P., "Characteristics of Flow in Falling Liquid Films," Chem. Eng. Prog., Vol. 48 pp. 557~563, 1952

(4) Rohsenow, W.M., Webber, J.H. and Ling, A.T., "Effect of Velocity on Laminar and Turbulent-Film Condensation," Trans. ASME, pp. 1637~1643, 1956

(5) Linehan, J.H., "The Interaction of Two-Dimensional, Stratifed, Turbulent Air-Water and Steam-Water Flows," Ph. D. Thesis, Dept. of Mech. Eng., Univ. of Wisconsion, 1968

(6) Brauer, H., "Stromung und Warmeubergang bei Rieselfilmen," VDI-Forschungsheft, 457, 1956

(7) Brotz, W., "Uber die Vorausberechnung der Absorptions-geschwindigkeit von Gasen in Stromenden Flussigkeitsschichten," Chemie-Ing.-Tech., 26, pp. 470~478, 1954

(8) Feind, K., "Stromungsuntersuchungen bei Gegenstrom von Rieselfilmen und Gas in Lotrechten Rohren," VDI-Forschungshaft, 481, 1960

(9) Zhivaikin, L. Ya. and Volgin, B.P., Zh. Prikl. Khim. 34, p. 1936, 1961

(10) Takahama, H., Fujita, H., Kodama, T., Kuribayashi, M. and Aiso, T., "Heat and Mass Transfer in Countercurrent Flow of Air and Water Film in a Rectangular Vertical Duct," Bull. of JSME, Vol. 17, No. 109, pp. 928~935, 1974

(11) Fulford, G.D., "The Flow of Liquids in Thin Films," Advances in Chemical Engineering, Vol. 5, Academic Press, New York, 1964

(12) Calvert, S. and Williams, B., "Upward Cocurrent Annular Flow of Air and Water in Smooth Tubes," AIChE J., Vol. 1, pp. 78~86, 1955

(13) Bankoff, S.G. and Kim, H.J., "Local Condensation Rates in Nearly Horizontal Stratified Countercurrent Flow of Steam and Cold Water," AIChE Symposium Series, Vol. 79, No. 225, pp. 209~224, 1983

(14) Collier, J.G. and Hewitt, G.F., "Film Thickness Measurements," AERE-R4684, 1964

(15) Hewitt, G.F., Measurements of Two Phase Flow Parameters, Academic Press, New York, 1978

(16) Kim, H.J. and Bankoff, S.G., "Local Heat Transfer Coefficients for Condensation in Stratified Countercurrent SteamWater Flows," J. of Heat Transfer, ASME, Vol. 105, pp. 706~712, 1983